lubricants

Article

Correlation of Tribological Behavior and Fatigue Properties of Filled and Unfilled TPUs

Chao Wang [1,*], Tanja Stiller [1], Andreas Hausberger [1], Gerald Pinter [2], Florian Grün [3] and Thomas Schwarz [4]

1 Polymer Competence Center Leoben GmbH, Roseggerstraße 12, 8700 Leoben, Austria
2 Chair of Materials Science and Testing of Polymers, Montanuniversität Leoben, 8700 Leoben, Austria
3 Chair of Mechanical Engineering, Montanuniversität Leoben, 8700 Leoben, Austria
4 SKF Sealing Solutions Austria GmbH, 8750 Judenburg, Austria
* Correspondence: c.submission.w@gmail.com; Tel.: +43-3842-42962-85

Received: 6 June 2019; Accepted: 17 July 2019; Published: 20 July 2019

Abstract: For a long service time, fatigue has been a typical problem that mechanical sealing materials face. How does it relate to tribological performance? In this study, filled and unfilled thermoplastic polyurethanes (TPUs) were investigated. Dumbbell and faint wait pure shear (FWPS) specimens were used to characterize the fatigue properties and crack growth rate of TPUs, respectively. Additionally, to identify the impact of temperature on fatigue tests, the tests were conducted at room temperature and 80 °C. Different tribological tests were conducted to investigate their tribological properties. Fracture surfaces from fatigue tests and worn surfaces from tribological tests were analyzed using a scanning electron microscope (SEM). Two wear models were verified to correlate between fatigue and tribological properties; one of the models is better for rough counter surfaces, while the other is advantageous if the counter surface is smooth.

Keywords: fatigue; filler; TPU; tribology; crack

1. Introduction

Thermoplastic polyurethane (TPU) is an elastomer that is also fully thermoplastic. Due to these unique properties, TPU compensates for the material gap between rubbers and plastics. As a linear segmented block copolymer, TPU consists of hard and soft segments [1]. By varying the ratio and types of these segments, TPU can provide exceptional flexibility in its properties, making it an ideal polymer in many applications. With good strength, excellent abrasion, and tearing resistance, TPU has also been applied recently as a mechanical seal. When mixed with fillers, its properties can be enhanced [2]. Nguyen et al. [3] investigated the functionalized graphene sheet as a filler in TPU, showing that the TPU matrix was efficiently reinforced, especially in the temperature region above the soft segment melt. A multiwalled carbon nanotube-graphene hybrid as a filler in TPU was studied by Roy et al. [4]. More than 200% improvement of storage modulus in the rubber state can be achieved. Suresha [5] researched the friction and dry sliding wear of short glass fiber (SGF) reinforced TPU. He found that the coefficient of friction decreases with increasing SGF content in TPU, and 40 wt% of SGF in TPU shows the best tribological performance for a bearing application. Mineral fillers have also been investigated. Barick et al. [6] studied the effect of organoclay nanocomposites on TPU's thermal and dynamic mechanical properties and found that storage modulus, loss modulus, and glass transition temperature are significantly increased with increasing nanoclay content to 9 wt%. The effect of mica and aluminum trihydrate as fillers in TPU were studied by Pinto et al. [7]. With 20 phr of mica, the best reinforcement effect was achieved regarding tensile strength, whereas a high amount of aluminum trihydrate provides good flame resistance, but causes a pronounced decrease in tensile strength, abrasion resistance, and hardness. However, few researchers have addressed the effect of fillers on fatigue or tribological properties in TPU.

In this work, we try to bridge this gap and present a possible correlation between fatigue and tribological properties for graphite-filled and unfilled TPUs. To characterize the basic mechanical properties, tensile tests and a dynamic mechanical analysis were performed. Notched dumbbell samples were applied to investigate the fatigue properties, and notched pure shear specimens were used to analyze the crack growth behavior. The tribological properties were studied through component-like tests. The influence of the load was determined by load ramp tests and the influence of counterpart roughness by different ground steel discs. Both fracture surfaces of fatigue tests and worn surfaces from tribological tests were analyzed with scanning electron microscopy (SEM).

2. Experimental Details

2.1. Material

The TPU specimens were produced by injection molding at SKF Sealing Solutions Austria GmbH. Two kinds of TPUs were studied, namely unfilled TPU (TPU_A) and graphite-filled TPU (TPU_B). The hardness was measured using the Shore D method, according to the standard DIN ISO 7619-1 [8]. The density was measured using a level balance (Mettler–Toledo, Columbus, OH, USA) using the buoyancy method—Archimedes' principle. The tensile tests were conducted with ISO 527-2 standard [9] test specimens (S2) with 200 mm/min on a Zwick Z010 (Zwick GmbH, Ulm, Germany). In order to get a wide range of temperature dependence of material properties, two temperatures (23 °C, 80 °C) were chosen for the tensile and fatigue tests. 23 °C is the room temperature and 80 °C is the average contact temperature in the tribological experiments. Due to the friction heat, the temperature in the contact interface increased significantly, while in the fatigue test the temperature increase was less than 5 °C. Therefore, the fatigue tests at 80 °C were conducted to obtain the fatigue behavior at a high temperature and a better understanding and correlation between fatigue and tribological properties. The dynamic mechanical properties were analyzed by means of dynamic mechanical analysis (DMA) utilizing the temperature scan method (EPLEXOR 100 N, NETZSCH GABO Instruments GmbH, Ahlden, Germany). Concerning the thermal influence on the samples, thermal conductivity was measured with a guarded heat flow meter (DTC 300, TA Instruments, New Castle, DE, USA) at 25 °C. Hardness measurements were repeated five times, and other experiments were repeated three times with similar results. The material properties are shown in Table 1.

Table 1. Material properties of the thermoplastic polyurethanes (TPUs) used in this study.

	Shore D	Density [g/cm^3]	Thermal Conductivity [W/mK]	Dynamic Mechanical Analysis (2Hz)			
				Temperature [°C]	Storage Modulus [MPa]	Loss Modulus [MPa]	Loss Factor
TPU_A	46 ± 0.71	1.196 ± 0.001	0.209 ± 0.001	23 80	100.07 ± 6.87 42.08 ± 0.36	17.68 ± 2.10 1.74 ± 0.09	0.1763 ± 0.009 0.0413 ± 0.0018
TPU_B	49 ± 1.58	1.225 ± 0.001	0.229 ± 0.001	23 80	110.97 ± 7.37 47.57 ± 0.34	19.70 ± 2.37 1.95 ± 0.10	0.1771 ± 0.0095 0.0410 ± 0.0018

2.2. Wear Prediction Model

In this study, two wear models were applied to correlate the wear behavior and fatigue properties. The first model, developed by Panda [10], is based on abrasive and fatigue wear mechanisms. In Panda's model, the surface roughness of the counter surface is taken into consideration. It is possible to predict the influence of roughness on wear. The second model was developed by Atkins et al. [11]; it is based on the adhesive and fatigue wear mechanisms and is able to correlate the wear rate with the number of cycles until failure.

2.2.1. Panda's Model

Description of Model

In Panda's model, wear is partly due to the fatigue wear mechanism, which is purely caused by elastic contacts, while the other part is from the abrasive mechanism under plastic contacts [10,12]. The model is based on the micro-mechanistic deformation at the asperity scale. Therefore, it is assumed that the interface consists of an ideally smooth polymer surface and a random rough counter surface. The asperities on a rough surface are rigid and show a spherical tip; they follow a probability distribution. In addition, abrasive wear only results from plastic contacts of asperities, while only elastic contacts lead to fatigue wear [10]. The filler effect, specimen roughness, and thermal influence are beyond the scope of this model.

The abrasive wear can be described as

$$V_a \approx N_s\left(\frac{\pi^2\mu H^2\overline{R}^2\sigma^4}{K_{IC}^2}\right)\int_{\Delta_2}^{\infty}(f_A)^3\varnothing(h+\Delta)d\Delta \tag{1}$$

$$f_A = 2\Delta^{2/3} - \frac{\Delta_c}{\Delta^{\frac{1}{3}}} - \frac{2}{\lambda\Delta^{1/3}},\ N_s = \eta A_s \tag{2}$$

where:

- N_S: Total number of asperities encountered during sliding;
- η: Average asperity density per unit area in μm^{-2};
- A_s: Total area covered during the tribological test in μm^2;
- μ: Coefficient of friction;
- H: Hardness in MPa, coverted from Shore D;
- $\overline{R}$: Average radius of curvature at asperity tip in μm;
- σ : Standard deviation of asperity heights in μm;
- K_{IC} : Fracture toughness MPa·m$^{0.5}$;
- h : Normalized mean separation in μm;
- Δ : Normalized deformation in μm;
- $\Delta_{c:}$ Critical normalized deformation;
- λ :$H\sigma/\gamma$ [13];
- γ : Surface energy per unit area J·m^{-2}.

The fatigue wear can be calculated with

$$V_f \approx N_s\left(\frac{1.5C\Psi}{\pi}\right)\int_{\Delta_0}^{\Delta_1}V_{el}(f_F)^t\varnothing(h+\Delta)d\Delta \tag{3}$$

$$C = \frac{\pi\mu(4+\nu)}{8} + (1-2\nu)/3,\ \Psi = \left(\frac{K}{H}\right)\sqrt{\sigma/R} \tag{4}$$

$$f_F = \sqrt{\Delta} - \sqrt{\Omega - \sqrt{\Delta}},\ \Omega = (6\pi/\theta)\sqrt{R/\sigma} \tag{5}$$

The volume of deformation under elastic contact can be described as

$$V_{el} = \pi\left\{\overline{R}\Delta^2 - \left(\Delta^3/3\right)\right\}\sigma^3,\ \Delta \leq \Delta_{el} \tag{6}$$

where:

- ν: Poisson's ratio;
- K: Combined Young's modulus of two surfaces in MPa;

- *t:* Fatigue ratio;

The total wear volume is a summary of both parts:

$$V \approx \alpha V_a + V_f \tag{7}$$

where: α: Factor for abrasive wear.

A factor was introduced for abrasive wear. It is assumed in the model that the ideal smooth polymer surface slides against a rough counter surface all through the tests. However, in real tribological tests, a transfer film is formed after the running-in phase [14–16]. Hence, the interface changes and the abrasive wear are not the dominant wear mechanisms. Especially for filled polymers, fillers can significantly affect the wear rate through the transfer film [14]. The factor α is defined as a ratio of the duration of the running-in phase and whole test duration, obtained from tribological tests.

Parameter Generation

The hardness was measured with a Shore D hardness tester. The fracture toughness and fatigue ratio were obtained from dumbbell tests. In terms of surface parameters, the counter surfaces were characterized according to the standard [17] with a 3D optical microscope (InfiniteFocus, Alicona Imaging GmbH, Raaba, Austria). Based on the surface measurements, the surface parameters were calculated using MATLAB programs (ver. 2018b). The determination of surface energy was carried out in a self-developed contact angle device. The methods of Owens et al. [18], Rabel [19], and Kaelble [20] were employed to calculate the surface energy.

Experimental Deatils

The fatigue tests were conducted with dumbbell specimens on a dynamic mechanical analyzer (ElectroForce 3450, TA Instruments, New Castle, DE, USA). The tests were carried out in the load-controlled mode with a sinusoidal signal. The frequency used was 3 Hz, which is a compromise of test duration and thermal influence. The specimen geometry is shown in Figure 1. In the middle of the specimen, a sharp circumferential initial notch (depth ≈ 1 mm) was introduced using a razor blade (thickness = 0.1 mm, tip radius <5 mm), which was mounted on a lathe. After the tests, the area of the fracture surfaces was measured with optical microscopy (Stereo Microscope SZX 12, Olympus, Tokyo, Japan). The calculation of the stress was based on the fracture surface measured. To investigate the influence of the temperature on the fatigue property of unfilled and filled TPUs, tests were conducted at room temperature (23 °C, 50% RH) and 80 °C.

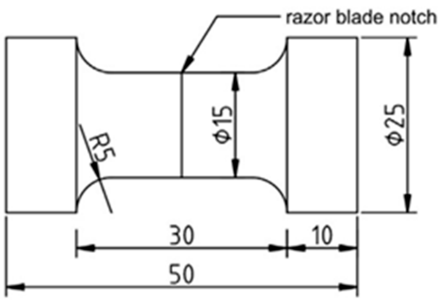

Figure 1. The geometry of a specimen used for fatigue [21].

Distilled water and diiodomethane were applied as liquids to determine the polar and dispersive parts of the surface energy, respectively. For each measurement, a drop with 2.5 µL volume was used. Each measurement was repeated three times.

A pin on disc configuration was used to investigate the influence of the counterpart roughness. The tests were conducted on a Universal Mechanical Tester (UMT-2, Bruker Nano Surfaces Division, Campell, CA, USA) with a rotating steel disc as the counterpart, made of 100Cr6 with a roughness

(R_a) of 0.3 µm or 0.03 µm. The roughness was characterized, according to the standard [17], with a 3D optical microscope (InfiniteFocus, Alicona Imaging GmbH, Raaba, Austria). The sample slid on a counter surface at 150 mm/s for 4 h. The total track length for each test was 2.16 km. All experiments were repeated three times with similar results.

2.2.2. Atkins Model

Based on a publication of Omar, Atkins, and Lancaster [9], the model aims to find a mathematical correlation of tribological values and fatigue values.

Description of Model

Atkins et al.'s [11] idea to correlate the wear and crack growth behaviors of the same material was revived and adapted for TPU [22]. Atkins investigated the correlation of different thermoplastics in a dry or wet state. The basic equation (Equation (1)) is the Paris–Erdogan law, which sets the correlation between the stress intensity factor and the crack growth rate. The Paris–Erdogan law is solved based on the cycle number. Atkins' idea was to correlate the wear rate with the inverse value of the number of cycles until failure, as demonstrated in Equation (9).

$$\frac{da}{dN} = A * K^n \tag{8}$$

$$Wear\ rate \propto \frac{1}{N_f} \propto A * \Delta\sigma^n * \sqrt{\pi^n} * a_0^{\frac{n}{2}-1} * \left(\frac{n}{2} - 1\right) \tag{9}$$

where:

- *a:* Crack length (a_0 initial crack length);
- *N:* Cycle number;
- *A:* Material constant;
- *K:* Stress intensity factor;
- *n:* Slope of the straight;
- *Δσ:* Difference in applied stress.

For the calculation of a theoretical wear rate, there is the need for some values, which can be calculated using the data from the experiments. N_f is the fatigue cycle number at which the specimen breaks. The value a_0 can be correlated to the wear particle thickness. For Equation (9), the stress intensity factor K is substituted by $\Delta\sigma(\pi a)^{1/2}$. All these assumptions were put in the Paris–Erdogan law, integrated, and then solved to the fatigue cycle number.

Since the model was made with polyethersulphone (PES) and polymethylmethacrylate (PMMA), it was tested with single edge notched specimens. Due to the elasticity of TPUs, it is not recommended that the same geometry be used, because of the deformation in front of the crack tip [23]. To use this geometry, a J-integral would be necessary to calculate the required values. Another way of calculating them is to use a pure shear specimen. This geometry allows the energy release rate to be substituted with the tearing energy [21]. Because of the proportionality of the energy release rate and stress intensity factor, including the E-modulus and Poisson's ratio, it is valid to substitute the stress intensity factor with

$$G = -\frac{dU}{dA} = -\frac{U}{t * (L - da)} = Wh_0 = T \tag{10}$$

where:

- *G:* Energy release rate in J/m^2;
- *U:* Energy required for crack growth (area under σ-ε curve) in J;
- *A:* Uncracked surface of specimen in mm^2;
- *t:* Thickness of specimen in mm;

- *L:* Initial length of uncracked area in mm;
- *a:* Crack length in mm;
- *W*: Work of cracking in N/mm^2;
- h_0: Constant height of the testing area in mm;
- *T:* Tearing energy in J/m^2.

The tearing energy *T* or energy release rate *G* describes the required energy to provoke an ongoing crack. *G* represents the released energy *U* by the newly-formed area *A*, which can be written as the thickness *t* of the specimen and the ongoing crack length *da*. For elastomers, the Paris–Erdogan law is valid for a stable crack growth region and can be written as Equation (11). For a calculated wear rate based on the mechanical fracture values, the tearing energy is calculated by the energy *U* divided by the remaining area of the surface. This term is put into the Paris–Erdogan law and solved after the crack length with the following, Equation (12).

$$\frac{da}{dN} = B * T^m \tag{11}$$

$$a_0 = L - \sqrt[m+1]{N * B * (m+1) * \left(\frac{U}{t}\right)^m} \tag{12}$$

where:

- *B:* Material constant in mm/cycle;
- *m:* Slope of the straight [–];
- a_0: Initial crack length at which wear particles start to detach in mm.

To get a minimal crack length, the values were used after the first 1000 cycles. This crack length was taken to calculate a fatigue cycle number by solving the Paris–Erdogan law. An assumption here is a continually growing crack, which means it always cracks at the same length.

Parameter Generation

To set up the Atkins model, tribological and fracture mechanical tests were conducted to generate the necessary values.

Tribological Values

For the correlation, two different kinds of test setup were used; a Ring on Disc (RoD) with different load levels and a Pin on Disc (PoD) with different counterpart roughness. These investigations generated the necessary wear rate, which will be correlated with a calculated wear rate. These values are calculated with the weight loss, applied load, and test distance.

Crack Growth Tests

The necessary parameters can be measured from the crack growth tests, which provide all values to calculate an initial crack length. This crack length can be taken to calculate a fatigue cycle number if a crack is growing equidistantly. *L* and *t* are just geometrical values, *N* is the fatigue cycle number of a certain load level, and *B* and *m* are determined by the curves of the tearing energy over the crack growth rate. *U* is the integrated force displacement or stress-strain curve.

Experimental Details

Tribological Investigation

To determine the wear rates, a Universal Mechanical Tester (UMT-2) (Bruker Nano Surface Division, Campell, CA, USA) and a TE93 Precision Rotary Tribometer (Phoenix Tribology Ltd., Berkshire, England) were utilized. An investigation of roughness influence was performed on the UMT-2, whereas the load ramp tests were done on the TE93. For each test setup, the counterparts were made of 100Cr6 steel and the roughness was controlled according to [17].

The PoD tests were conducted with a rotating speed of 150 mm/s at a load of 1 MPa for 4 h, later shortened by UMT-2 rot. To compre between both test setups, the RoD tests were conducted at 150 mm/s and 4 h of testing. To gain some information about the influence of the load, two different load levels were chosen, namely 1 MPa and 1.5 MPa. These load ramp tests were developed by Jölly for TPU materials [24]. The results of the load ramp were shortened by TE LR. For lower loads, the filler cannot evolve its lubricating potential [25]. Therefore, higher loads were chosen.

Crack Growth Investigations

To investigate the crack growth behavior, pure shear tests were conducted. To ensure a horizontally growing crack, faint waist pure shear (FWPS) specimens were tested. When using these slightly curved specimens, Equation (3) ($Wh_0 = T$) is not valid. However, the thickness was assumed to be constant, thus justifying that it should only provide information on the conductibility and a possible trend. The geometry of an FWPS specimen is illustrated in Figure 2.

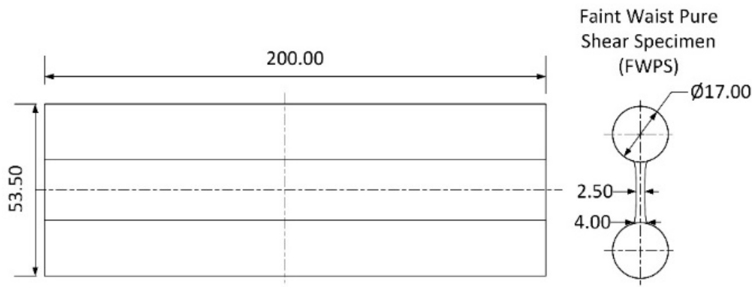

Figure 2. Geometry of a faint waist pure shear (FWPS) specimen for crack growth investigations.

The tests were conducted on an MTS 858 tabletop system (MTS Systems Corporation, Eden Prairie, MN, USA) and run in a load-controlled mode with a testing frequency of 3 Hz. The specimens were notched with a razor blade. The initial crack length was 25 mm, and the specimens were sprayed with a developer (Nord-test developer U89, Helling GmbH, Heidgraben, Germany) before testing for a higher contrast in photos, which facilitates the crack observability. To observe the crack growth, a camera system was employed, which took a picture every 1000 cycles. The crack growth was analyzed with a Tracker (version 5.0, comPADRE). The tests were performed with a stress ratio of 0.1 (F_{min}/F_{max}) at room temperature. These tests were conducted at an F_{max} of 2700 N and 3000 N. Lower loads took too long to crack, whereas higher loads led to too fast failure. The specimens were tested until they ripped completely apart in two halves, but for the evaluation only the first half of the cracking was considered, due to the undefined stress situation of a further cracked specimen [26,27].

3. Results & Discussion

Firstly, the results of the fatigue tests are discussed. The evaluation is based on the stress-cycle (S–N) curve, stress intensity factor, and dissipated energy. As one of the basic mechanical properties of materials, tensile tests at room temperature and 80 °C correlate well with fatigue tests. Secondly, crack growth tests are shown and correlated with the fatigue tests. The fracture surfaces show the crack growth processes. For tribological tests, the coefficient of friction (COF) and wear rate are discussed. The surfaces after the tests are analyzed and discussed.

3.1. Comparison of Two Materials

3.1.1. Fatigue Tests

Stress–Cycle (S–N) Curve

The S-N curve is shown in Figure 3. In order to achieve a better correlation with tensile tests, maximum stress σ_{max} is plotted as the y-axis (logarithmic) against the number of cycles to failure (logarithmic).

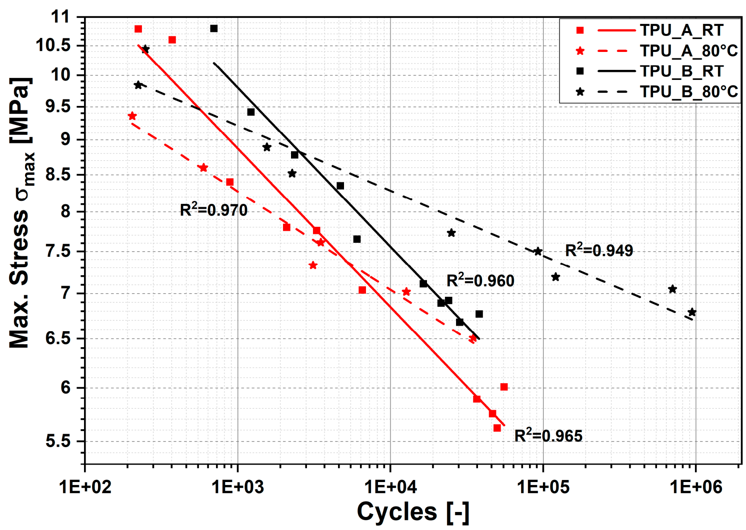

Figure 3. The stress–cycle (S–N) curve of the tested materials.

In this study, the cycles to failure follow a power law

$$N = \left(\frac{\sigma_a}{\sigma_0}\right)^k \tag{13}$$

where N is cycles to failure, σ_a is the maximum stress, and σ_0 and k are constant. As shown in Figure 3, the curves of both materials at room temperature are parallel, indicating that fillers in TPU_B are beneficial for these kinds of fatigue tests at room temperature. However, the reinforcement effect of the filler against fatigue is not because fillers strengthen the crack growth resistance of TPU_B, but rather because they increase the E-modulus. Under the same conditions, TPU_B experienced approximately double the time to fail as TPU_A.

For the tests at room temperature, at low load, the S–N curve corresponds very well with the stress-strain curve. There is evidence to indicate that in the S–N curve, the stresses at the same cycles to the failure can be traced back to the same strain in the tensile test. This implies that at the low load, the key factor that influences the cycles to failure is the strain. Even though TPU_B is filled, it has the same lifetime as TPU_A when the tests are conducted with the same strain. At the high load, due to the stronger nonlinearity of the tensile curve, the correspondence is not as good as at the low load. However, the trend can still be identified.

At elevated temperature, the slope of the curves becomes slight. There is a cross point of the curve at room temperature and 80 °C for each material. It indicates that, compared to the tests at room temperature, the fatigue properties of the two materials are more sensitive to the load at elevated temperature. The cross point for TPU_A is about 7.4 MPa, while for TPU_B it is 8.8 MPa. At cross points, the positive and negative effects of elevated temperature on fatigue properties balanced out. For both materials, when the maximum stress is higher than the cross-point stress, elevated temperature represents an adverse effect on the fatigue property. At lower stress, a high temperature brings advantages to fatigue properties.

Stress Intensity Factor

The stress intensity factor ΔK_I was calculated according to Benthem and Koiter [28]. Both materials show a linear trend at room temperature, while at elevated temperature the linear trend shows a more significant deviation compared to the trend at room temperature (Figure 4). In general, the trends correspond well with those in the S–N curve. This indicates that in the tests, the total maximum stress is more relevant to predict the lifetime of the samples.

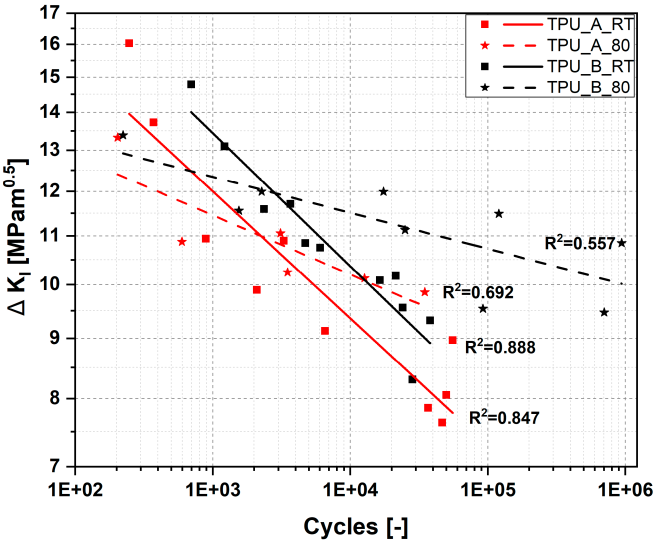

Figure 4. Stress intensity factor of the tested materials.

3.1.2. Crack Growth Tests

Tearing Energy Over Cycles

In Figure 5a, the tearing crack growth rate is plotted against the tearing energy. This kind of plotting provides information about the crack growth resistance by analyzing the slope of the graphs. A higher slope means a lower resistance against crack growth. It is visible that TPU_B has a lower crack growth rate than TPU_A, which can be traced back to the higher stiffness due to the filler. The high scattering of the values at the beginning of the curves is due to the barely recognizable crack growth in the evaluation of the pictures. After a certain crack length, the curves separate clearly.

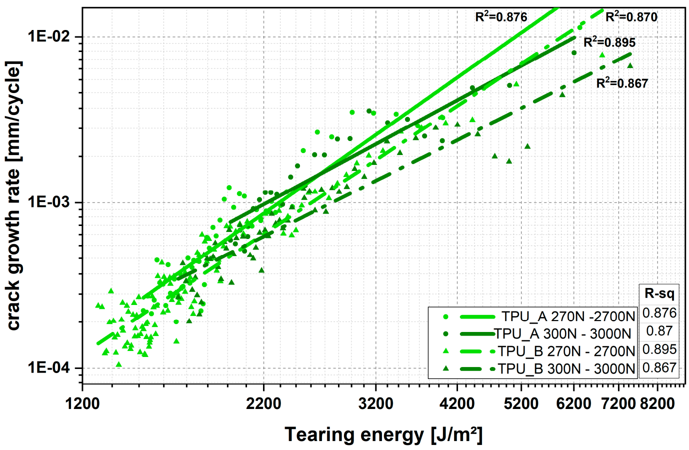

(**a**)

Figure 5. *Cont.*

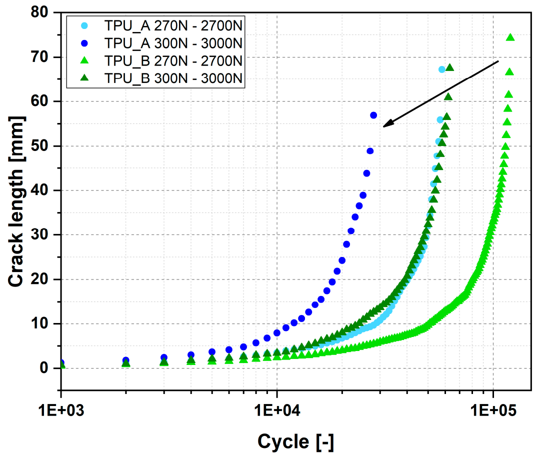

(**b**)

Figure 5. (**a**) Tearing energy plotted against the crack growth rate of unfilled TPU (TPU_A) and graphite-filled TPU (TPU_B) for 270–2700 N and 300–3000 N; (**b**) the average crack length after every 1000th cycle for the same loads.

The higher crack growth resistance is evident if the crack length is examined over the cycles, as shown in Figure 5b. In this plot it is visible that TPU_A continues to crack earlier than TPU_B. It is also visible that under tearing energy of approx. 2400 J/m^2, no significant separation can be observed. The values are not usable if the crack reaches the half-length of the specimen, since, theoretically, under those conditions, the shear is not pure shear anymore [27]. For the FWPS tests, the impact of temperature was studied by Schieppati et al. [29], which shows that a higher local strain leads to an increase in temperature at the crack tip.

3.1.3. Tribological Tests

For tribological tests, the real contact stress at the contact point is much higher than the nominal contact stress.

Load Ramp Tests

The results of load ramp tests are shown in Figure 6. The COF and average contact temperature are only calculated for each load ramp stage, while the weight loss is determined for all of the previously experienced stages. Generally, COF decreases with load increments, while a higher load leads to more weight losses. This result is in good agreement with Schallamach's research [30], which is based on the real contact area combined with Hertz's contact theory. When increasing normal load, more asperities come into contact. However, COF, which is mainly determined by the contact state between the two rubbing surfaces, is affected by many other factors, e.g., temperature, wear debris in between, material properties at elevated temperature, fillers, etc. The contact state changes continuously with cycles.

When the load is 0.5 MPa, both materials behave similarly, which indicates that at a low load, the beneficial effect of fillers cannot be manifested noticeably. As the tests run further to the next stage, COFs decrease rapidly; for TPU_A the reduction of COF is ca. 12%, while for TPU_B it is over 35%. The contact temperature of TPU_A increased from 82 °C to 115 °C, whereas the contact surface of TPU_B experienced a declining temperature from 91 °C to 62 °C as the load increased to 1 MPa. This can be attributed to two factors. One crucial point is that heat was generated by friction. Since the COF decreases significantly for TPU_B, the work, which was converted into thermal energy, reduced consequently. In addition, thermal energy can be taken away from the contact surface by wear debris. The wear volume increased considerably for TPU_B, while for TPU_A its wear volume remained almost unchanged. Thermal energy was accumulated to heat the whole system, including the sample, counterpart, holders, drive shaft, etc. With increasing time, the system got heated and stayed in a relatively balanced state.

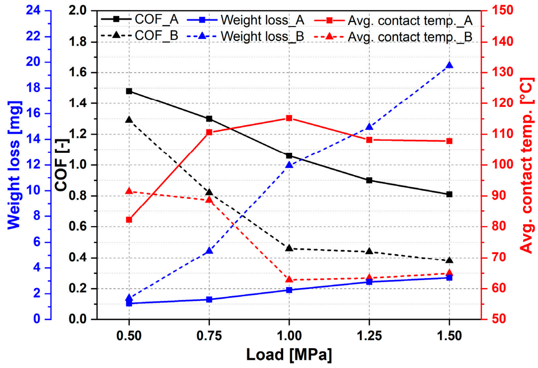

Figure 6. Results of load ramp tests of TPU_A and TPU_B.

Both COFs decreased when the load increased to 1 MPa. Significant weight loss was observed for TPU_B, while it stayed almost unchanged for TPU_A. For TPU_B, this load is an inflection point. After this stage, its COF and contact temperature kept stable, though its weight loss increased more or less proportionally to the load. For TPU_A, it seems that its contact temperature reaches a balance at this stage. It decreases at the next stage as a result of the reduction of COF. A slight increase in wear can be identified through 1.5 MPa.

Table 2 shows the worn surface of the load ramp tests of TPU_A and TPU_B. After the first stage (0.5 MPa), the texture from turning marks is still visible in the whole contact area. The peaks of the turning textures become relatively flat. The height difference between the peak and the middle of the groove, however, is still visible. By contrast, rolled worm-like debris can be observed on TPU_B, especially on the peaks of the turning textures. This phenomenon can also be found in [31,32]. This phenomenon occurred in the outer area of TPU_A at higher loads. Due to the effect of time and higher normal stress, after the second stage, the turning textures could still be identified, but the peaks were almost worn out. TPU_B experienced serve rolled wear so that the turning textures could not be observed after the tests. In some places, fillers were uncovered due to wear debris. Fillers were uncovered after the substrate polymer was "smeared", due to sliding movement. However, the filler system starts to show its effect. As can be seen in Figure 6, a significant change occurred for TPU_B under 1 MPa normal load. The COF and contact temperature decreased with an increase in wear volume. At this stage, a transfer film was generated. Thus, the interface changed from metal-TPU to graphite-graphite. The transfer film was not perfect and covered the whole contact area. After this stage, TPU_B reached a relatively stable stage. When increasing the normal load, its COF stayed at the same level. The wear volume, however, kept increasing. Under a higher normal load, adhesive wear dominated in TPU_A.

Table 2. Scanning electron microscope (SEM) micrographics of load ramp tests of TPU_A and TPU_B.

	TPU_A	TPU_B
0.5 MPa	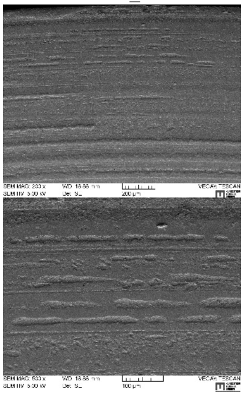	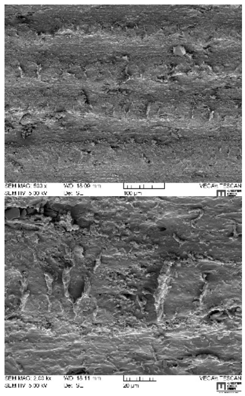
1.0 MPa	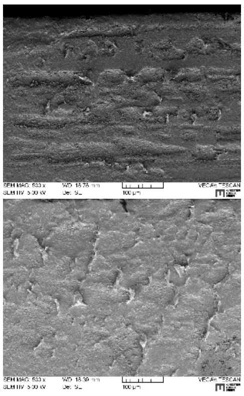	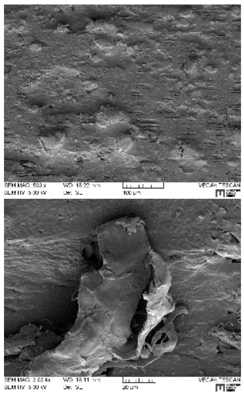
1.5 MPa	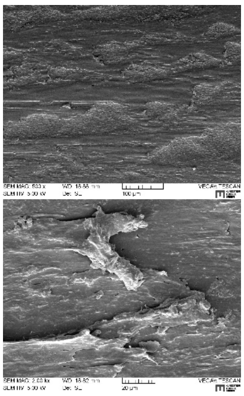	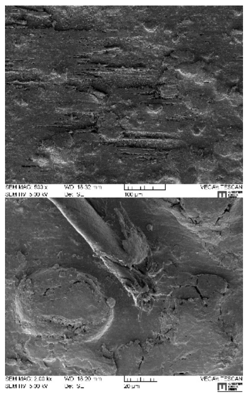

Pin on Disc Tests

To check the influence of counterpart roughness, the steel discs were prepared in a smooth (R_a = 0.03 µm) and a rough (R_a = 0.3 µm) way. Besides the roughness, all parameters are kept the same to have comparability between the two roughnesses without any other influences. In Figure 7, the coefficient of friction and wear rate for both roughnesses are shown. For TPU_B, due to the filler effect and stiffness, its average COF is lower than TPU_A for both roughnesses. Its higher stiffness facilitates a reduction of the deformation part of friction [33,34]. Higher wear rate was identified for both materials with a rough counter surface. However, probably due to the tribologically advantageous transfer film of TPU_B, its wear rate does not show a significant difference between rough and smooth counter surfaces. For TPU_A, its wear rate on the rough counter surface is higher than that with a smooth counter surface.

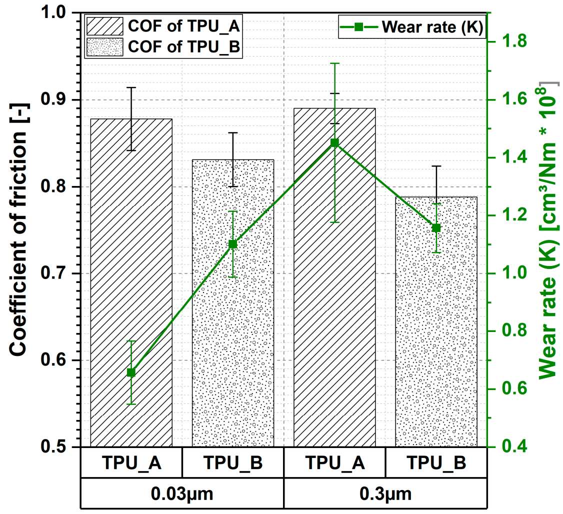

Figure 7. Coefficient of friction and wear rate (K) for TPU_A and TPU_B tested on different counterpart roughnesses.

3.2. Damage Analysis Proof

Since a comparison of different tests or dimensions needs proof, the damage of the surfaces should provide equivalency. If the appearance of the damage is comparable, it means the same failure process took place. In Table 3, all three mechanical tests with damage are summarized for both materials. The arrows indicate quite similar damage, which looks like waves for the mechanical fracture tests. This is caused by the cyclic loading, during which the material elongates relaxes relatively. Even though the tribological surface does not show such characteristic waves, it exhibits the same off ripping damage as for the fracture mechanical tests. The remaining part on the surface is immediately attached to the surface because of the contact with the counterpart, therefore no relaxing of the stripes is possible and no wave structures can be formed.

Table 3. Comparison of the damage equality of tribologically and mechanically fractured tested specimens.

	Tribo	Dumbbell	FWPS
TPU_A	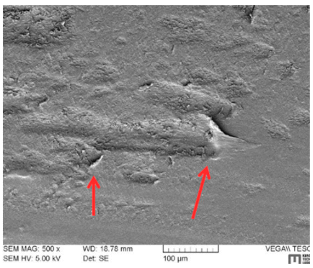	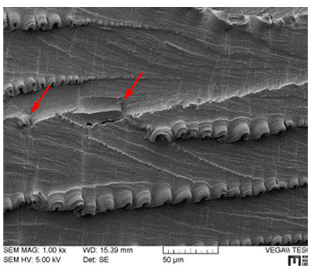	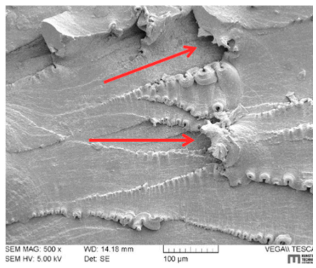
TPU_B	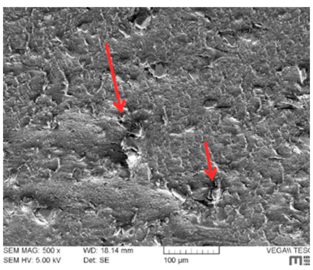	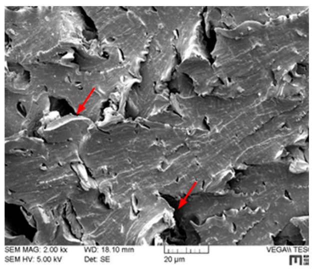	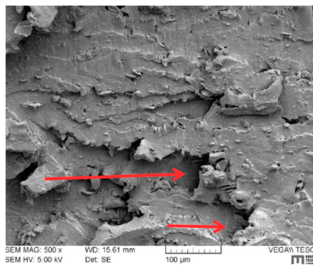

3.3. Verifications of Two Models

3.3.1. Panda's Model

The roughness parameters of two counterparts are shown in Table 4. In addition, the material properties were obtained through different tests and are shown in Table 5.

Table 4. Roughness parameters of two counterparts.

Surfaces	σ (µm)	R (µm)	η (µm^{-2})	Sk	Ku	β_{Sk}	β_{Ku}
Rough ground	0.68	1.211	7.39×10^{-4}	0.06719	2.988	1.39	0.88
Smooth polished	0.26	2.28	7.60×10^{-4}	−0.215	3.367	1.99	0.96

- ς: Standard deviation of asperity heights;
- R: Average radius of curvature at asperity tip;
- η: Average asperity density per unit area;
- Sk: Skewness of asperity heights;
- Ku: Kurtosis of asperity heights;
- β_{Sk}: Weibull shape parameter from skewness;
- β_{Ku}: Weibull shape parameter from kurtosis.

Table 5. Material properties of TPU_A, TPU_B, and counterpart.

Materials	E (MPa)	H (MPa)	S_y (MPa)	ν	K_{IC} (MPa m$^{0.5}$)	t	γ (J m^{-2})	ρ (g/cm^3)	α	
									Rough	Smooth
TPU_A	17.2 ± 0.2	37.04 ± 0.57	10.5 ± 0.1	0.48	7.8	2.2	0.033 ± 0.001	1.196 ± 0.001	0.0694	0.1389
TPU_B	19.6 ± 0.3	41.27 ± 1.14	12 ± 0.2	0.48	8.9	2.0	0.037 ± 0.001	1.225 ± 0.001	0.0694	0.1042
100Cr6 steel	2.1×10^5	710	500	0.28	-	-	-	7.9		

- E: Young's modulus;
- H: Hardness, converted from Shore D [35];
- S_y: Yield strength; for TPU, the stress at 50% strain from tensile test was used.
- ν: Poisson's ratio;
- K_{IC}: Fracture toughness; the minimum values from dumbbell fatigue tests were used.
- t: Fatigue ratio; based on the empirical research.
- γ: Surface energy;
- ρ: Density;
- α: Factor of abrasive wear.

Based on the values in Table 4; Table 5 and our tribological tests under the same conditions, wear rates were calculated. As shown in Figure 8, TPU_B has a better wear resistance to both counterpart roughnesses than TPU_A. However, in the experiments, only when it runs against a rough counterpart is the predicted trend consistent with the experimental results. For tests with a smooth counter surface, the predicted value is lower than the experimental results. This can be attributed to adhesive wear, which is included in this model, but for a smooth counter surface, especially when the transfer film is formed, adhesion turns out to be one of the primary wear mechanisms [12]. With a transfer film in the interface, abrasive wear can be reduced significantly. Moreover, as the blue line shows in Figure 8, for the rough counterpart, abrasive wear contributes to more than 96% of the total wear volume. For the tests with a smooth counter surface, abrasive wear is still dominant, but fatigue wear is higher than that with a rough counter surface.

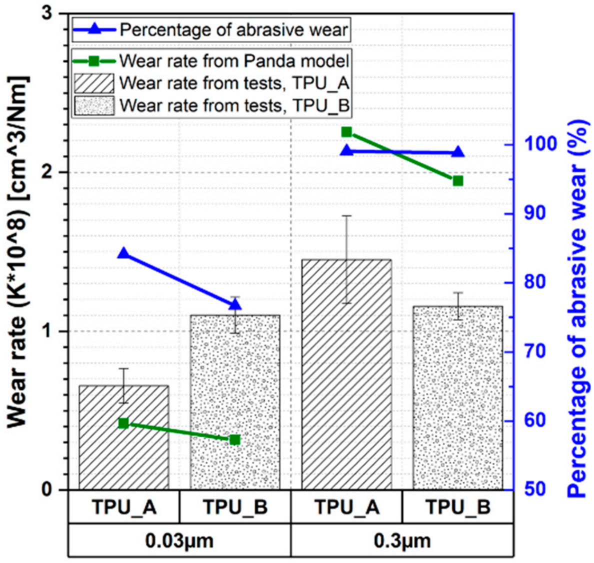

Figure 8. Comparison of wear rates from tests and analytical models.

3.3.2. Atkins Model

With all required parameters, the Atkins model can be used to compare tribological and mechanical fracture wear rates or fatigue cycle numbers, due to the correlation of wear rate $\propto 1/N_f$. The wear rate for the FWPS specimen was calculated in two ways; the first was the inverse value of the fatigue cycle number gained from the crack growth tests, and the second was calculating using the initial crack length, therefore determining a theoretical fatigue cycle number. The first method only includes the fatigue cycles, whereas the second also takes the mechanical fracture values into account. To check if the same trend is given for the dumbbell specimen, their fatigue cycle numbers for medium load levels were taken. In Figure 9, the comparison of the wear rates between the two investigated materials is plotted.

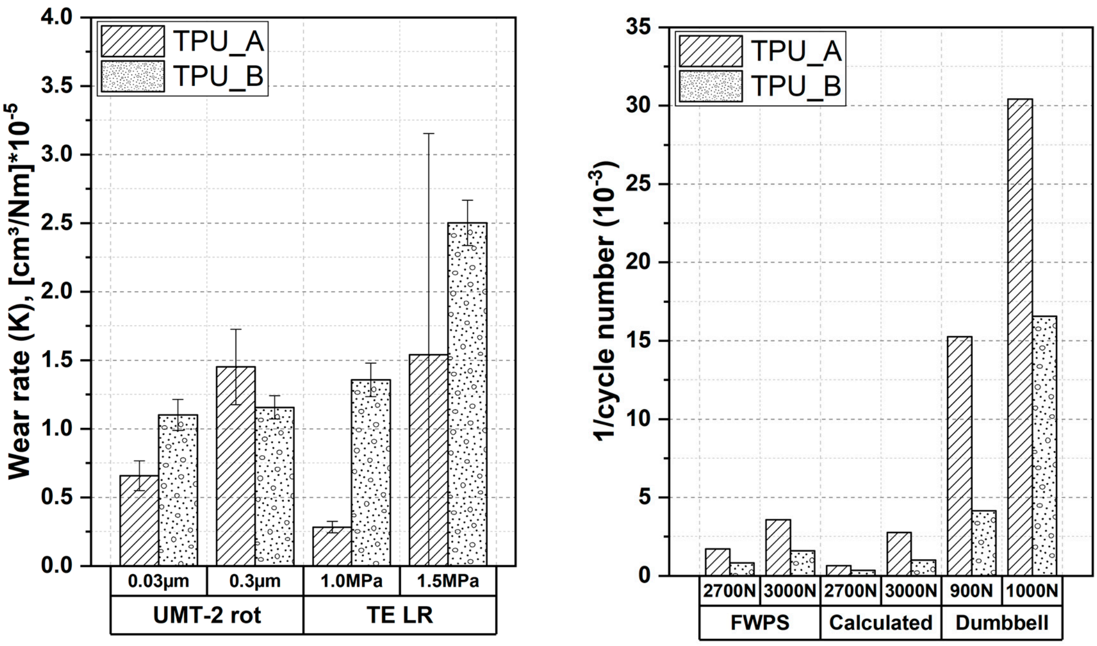

Figure 9. Comparison of the wear rates from the tribological and mechanical fracture tests of TPU_A and TPU_B for selected loads.

The depicted wear rates show a clear trend of higher wear rates for higher loads. Except for TE LR, the wear rate for TPU_A is higher than for TPU_B, the reason being the previously mentioned running-in wear, which is required to develop a transfer film on the counterpart. This fact can also be argued with the required tearing energy of 2400 J/m^2 to see a clear separation in Figure 5. It is possible that for both stressing types, mechanical and tribological, TPU_B needs a certain amount of energy or wear to develop its potential. This might be traced back to the filler, which acts to either stiffen or lubricate, depending on the mode of stressing. Even though TPU_B has a higher wear rate for the load ramp, the factor between the single loads and the counterpart roughness is smaller than for TPU_A. This includes the fact that TPU_B is less affected by higher stressing than the unfilled TPU_A. For mechanical testing, the inverse values of the fatigue cycle numbers were taken. The higher values of the wear rates calculated from the dumbbell specimen are due to the relatively small area of the specimen, which is more affected by higher loading. While the pre-notched area for a dumbbell specimen is around 130 mm^2, the area for a pre-cracked FWPS specimen is over three times higher, with 437.5 mm^2. Furthermore, it has to be mentioned that dumbbell specimens contain different stressing situations compared to the FWPS specimen.

3.3.3. Scope and Comparison of Both Models

Both models seem to cover one specific aspect of the tribological values. Panda's model shows a better fitting for rough surfaces, whereas Atkins' adapted model fits better for the smooth surfaces. This indicates that abrasive wear behavior should be explained using Panda's model, considering the roughness of both bodies. As already mentioned, as soon as a polymer film is developed on the counter surface, the model is no longer valid. On the other hand, a more adhesive wear mechanism can be described with Atkins' model, but only as a trend and not as a precise prediction.

4. Conclusions

In this study, a possible correlation between fatigue and tribological performance of unfilled und filled TPUs was found. This study also provides insight into the influence of filler on the fatigue and tribological properties of TPUs.

(1) Two models were verified to predict wear volume of filled and unfilled TPUs.
(2) The fatigue properties were identified with dumbbell tests. Fillers show a beneficial effect on the fatigue property at both temperatures. However, inverse impacts of temperature on low and high stresses were identified. The crack growth rate was characterized by means of faint waist pure shear tests. Filled TPU shows a better crack growth resistance.
(3) The tribological performance was characterized by various test configurations. An incubation period is necessary to generate a transfer film in the interface. Additionally, the influence of roughness of counterparts was identified.
(4) Similar failure mechanisms were identified in dumbbell, FWPS, and tribological tests.
(5) Panda's model shows a better prediction for the tests with a rough counter surface, while the Atkins model is advantageous to predict the results of the tests with a smooth counter surface. For the tests with a rough counter surface, abrasive wear contributes to more than 96% of the total wear, whereas for a smooth counter surface, abrasive wear is still the primary wear origin, but fatigue wear is about 20% of the total wear. Therefore, for a test, which model is better depends mainly on which wear mechanism is dominant. However, a lot of work still needs to be done to predict the wear precisely. Several factors, e.g., transfer film, temperature, etc., which are essential to wear generation, are not taken into consideration in this study.

Future work should focus on the temperature distribution and its effect on fatigue tests, and tribological tests have yet to be determined.

Author Contributions: Conceptualization, A.H. , C.W. and T.S.; Methodology, C.W. and T.S.; Validation, C.W. and T.S.; Formal Analysis, C.W. and T.S.; Investigation, C.W. and T.S.; Resources, Th. S.; Data Curation, X.X.; Writing-Original Draft Preparation, C.W. and T.S.; Writing-Review & Editing, A.H., G.P., F.G, Th.S.; Visualization, C.W. and T.S.; Supervision, A.H., G.P., F.G, Th.S..; Project Administration, A.H., Funding Acquisition, Th.S.

Funding: The present research was carried out at Polymer Competence Center Leoben GmbH within the framework of the Competence Center Program COMET by the Federal Ministry of Transport, Innovation, and Technology and the Federal Ministry of Economics, Family, and Youth, with the participation of the Chair of Mechanical Engineering and the Chair of Materials Science and Testing of Polymers, Montanuniversität Leoben, SKF Sealing Solutions Austria GmbH and also funded by federal and state governments of Styria, Lower Austria, and Upper Austria.

Acknowledgments: The authors thank B. Schrittesser, D. Fleischman, P. Marx, W. Balasooriya arachchige, J. Schieppati, and S. Agnelli for helpful discussions and advice.

Conflicts of Interest: The authors declare no conflict of interest.

References

1. Drobny, J.G. *Handbook of Thermoplastic Elastomers*, 2nd ed.; Elsevier: Amsterdam, The Netherlands, 2014; ISBN 9780323221368.
2. El-Sonbati, A.Z. *Thermoplastic Elastomers*; InTech: Rijeka, Croatia, 2012; ISBN 978-953-51-0346-2.
3. Nguyen, D.A.; Lee, Y.R.; Raghu, A.V.; Jeong, H.M.; Shin, C.M.; Kim, B.K. Morphological and physical properties of a thermoplastic polyurethane reinforced with functionalized graphene sheet. *Polym. Int.* **2009**, *58*, 412–417. [CrossRef]
4. Roy, S.; Srivastava, S.K.; Pionteck, J.; Mittal, V. Mechanically and Thermally Enhanced Multiwalled Carbon Nanotube-Graphene Hybrid filled Thermoplastic Polyurethane Nanocomposites. *Macromol. Mater. Eng.* **2015**, *300*, 346–357. [CrossRef]
5. Suresha, B. Friction and Dry Slide Wear of Short Glass Fiber Reinforced Thermoplastic Polyurethane Composites. *J. Reinf. Plast. Compos.* **2010**, *29*, 1055–1061. [CrossRef]
6. Barick, A.K.; Tripathy, D.K. Thermal and dynamic mechanical characterization of thermoplastic polyurethane/organoclay nanocomposites prepared by melt compounding. *Mater. Sci. Eng. A* **2010**, *527*, 812–823. [CrossRef]
7. Pinto, U.A.; Visconte, L.L.Y.; Reis Nunes, R.C. Mechanical properties of thermoplastic polyurethane elastomers with mica and aluminum trihydrate. *Eur. Polym. J.* **2001**, *37*, 1935–1937. [CrossRef]
8. Technical Committee ISO/TC 45 "Rubber and rubber products". *DIN ISO 7619-1:2012-02. Elastomere oder Thermoplastische Elastomere Bestimmung der Eindringhärte Teil_1: Durometer-Verfahren (Shore-Härte) (ISO_7619-1:2010)*; Beuth Verlag GmbH: Berlin, Germany, 2010.
9. Technical Committee ISO/TC 61/SC 2/WG 1 "Static behavior". *DIN EN ISO 527-2:2012-06. Kunststoffe Bestimmung der Zugeigenschaften Teil_2: Prüfbedingungen für Form-und Extrusionsmassen (ISO_527-2:2012), Deutsche Fassung EN_ISO_527-2:2012*; Beuth Verlag GmbH: Berlin, Germany, 2012.
10. Panda, S.; Sarangi, M.; Roy Chowdhury, S.K. An Analytical Model of Mechanistic Wear of Polymers. *J. Tribol.* **2018**, *140*, 11609. [CrossRef]
11. Omar, M.K.; Atkins, A.G.; Lancaster, J.K. The role of crack resistance parameters in polymer wear. *J. Phys. D Appl. Phys.* **1986**, *19*, 177–195. [CrossRef]
12. Chang, W.R.; Etsion, I.; Bogy, D.B. An Elastic-Plastic Model for the Contact of Rough Surfaces. *J. Tribol.* **1987**, *109*, 257–263. [CrossRef]
13. Fuller, K.N.G.; Tabor, D. The Effect of Surface Roughness on the Adhesion of Elastic Solids. *Proc. R. Soc. A Math. Phys. Eng. Sci.* **1975**, *345*, 327–342. [CrossRef]
14. Bahadur, S. The development of transfer layers and their role in polymer tribology. *Wear* **2000**, *245*, 92–99. [CrossRef]
15. Briscoe, B.J.; Sinha, S.K. Wear of polymers. *Proc. Inst. Mech. Eng. Part J J. Eng. Tribol.* **2002**, *216*, 401–413. [CrossRef]
16. Rhee, S.H.; Ludema, K.C. Mechanisms of formation of polymeric transfer films. *Wear* **1978**, *46*, 231–240. [CrossRef]
17. Technical Committee NA 152-03-03 AA "Surfaces". *DIN EN ISO 25178-1:2016-12. Geometrische Produktspezifikation_(GPS)_Oberflächenbeschaffenheit: Flächenhaft_Teil_1: Angabe von Oberflächenbeschaffenheit (ISO_25178-1:2016), Deutsche Fassung EN_ISO_25178-1:2016*; Beuth Verlag GmbH: Berlin, Germany, 2016.

18. Owens, D.K.; Wendt, R.C. Estimation of the surface free energy of polymers. *J. Appl. Polym. Sci.* **1969**, *13*, 1741–1747. [CrossRef]
19. Rabel, W. Einige Aspekte der Benetzungstheorie und ihre Anwendung auf die Untersuchung und Veränderung der Oberflächeneigenschaften von Polymeren. *Farbe und Lack* **1971**, *77*, 997–1005.
20. Kaelble, D.H. Dispersion-Polar Surface Tension Properties of Organic Solids. *J. Adhes.* **1970**, *2*, 66–81. [CrossRef]
21. Schrittesser, B. Performance of Elastomers for High-Pressure Applications. Ph.D. Thesis, University of Leoben, Leoben, Austria, 2014.
22. Stiller, T. InSitutribological and Fracture Mechanical Investigation of Thermoplastic Polyurethanes. Master's Thesis, Montanuniversität Leoben, Leoben, Austria, 2013.
23. Wang, C.H. *Introduction to Fracture Mechanics*; DSTO Aeronautical and Maritime Research Laboratory: Melbourne, Australia, 1996.
24. Joelly, I.A. Assessment of Contact Pressure and Sliding Velocity on the Tribological Performance of TPU SEAL Materials for the Establishment of a Rating System. Master's Thesis, Montanuniversität leoben, Leoben, Austria, 2011.
25. Stachowiak, G.W.; Batchelor, A.W. *Engineering Tribology*; Elsevier: Amsterdam, The Netherlands, 1993; ISBN 0-444-89235-4.
26. Stoček, R. Dynamische Rissausbreitung in Elastomerwerkstoffen. Dissertation, Technische Universität Chemnitz, Chemnitz, Germany, 2011.
27. Gdoutos, E.E.; Daniel, I.M.; Schubel, P. *Fracture Mechanics of Rubbe*; Socirety of Rubber Science and Technology Japan: Tokyo, Japan, 2003.
28. Benthem, J.P.; Koiter, W.T. Asymptotic approximations to crack problems. In *Methods of Analysis and Solutions of Crack Problems*; Sih, G.C., Ed.; Springer: Dordrecht, The Netherlands, 1973; pp. 131–178, ISBN 978-90-481-8246-6.
29. Schieppati, J.; Schrittesser, B.; Wondracek, A.; Robin, S.; Holzner, A.; Pinter, G. Impact of temperature on the fatigue and crack growth behavior of rubbers. *Procedia Struct. Integr.* **2018**, *13*, 642–647. [CrossRef]
30. Schallamach, A. The Load Dependence of Rubber Friction. *Proc. Phys. Soc. B* **1952**, *65*, 657–661. [CrossRef]
31. Grün, F.; Sailer, W.; Gódor, I. Visualization of the processes taking place in the contact zone with in-situ tribometry. *Tribol. Int.* **2012**, *48*, 44–53. [CrossRef]
32. Gódor, I.; Schiffer, J.; Grün, F.; Schwarz, T.; Major, Z. Tribological Behaviour of Unfilled and Filled TPU Materials. In Proceedings of the 14th Nordic Symposium on Tribology, Storforsen, Sweden, 8–11 June 2010; p. 59.
33. Hausberger, A.; Major, Z.; Theiler, G.; Gradt, T. Observation of the adhesive- and deformation- contribution to the friction and wear behaviour of thermoplastic polyurethanes. *Wear* **2018**, *412*, 14–22. [CrossRef]
34. Wang, C.; Hausberger, A.; Nothdurft, P.; Lackner, J.; Schwarz, T. The Potential of Tribological Application of DLC/MoS2 Coated Sealing Materials. *Coatings* **2018**, *8*, 267. [CrossRef]
35. Pampush, J.D.; Daegling, D.J.; Vick, A.E.; McGraw, W.S.; Covey, R.M.; Rapoff, A.J. Technical note: Converting durometer data into elastic modulus in biological materials. *Am. J. Phys. Anthropol.* **2011**, *146*, 650–653. [CrossRef]